Real-Time Micro-Raman Measurements on Stressed Polyethylene Fibers. 1. Strain Rate Effects and Molecular Stress Redistribution

P. A. Tarantili,[†,‡] A. G. Andreopoulos,[†,‡] and C. Galiotis*[,‡,§]

Department of Chemical Engineering, National Technical University of Athens, 9 Iroon Polytechniou Str., 157 80 Zografou, Athens, Greece, Department of Materials, Queen Mary & Westfield College, Mile End Road, London E1 4NS, U.K., and Institute of Chemical Engineering and High Temperature Chemical Processes, Foundation of Research and Technology−Hellas, P.O. Box 1414, GR 26500, Patras, Greece

Received October 9, 1996; Revised Manuscript Received April 21, 1997

ABSTRACT: The molecular deformation of ultrahigh-molecular-weight polyethylene monofilaments was monitored in real time by remote laser Raman microscopy (ReRaM). A shift to lower wavenumbers of the symmetric and asymmetric C−C stretching mode bands, was observed in agreement with previously published data. The stress or strain dependence of the Raman wavenumbers as a function of strain rate was also examined at room temperature. Furthermore, the broadening of the Raman bands as a function of applied stress or strain was investigated and compared with the wavenumber shift in each case. The Raman band shift for the asymmetric and symmetric C−C stretching modes per stress or strain was found to be only marginally affected for strain rates ranging from 10^{-4} to 10^{-3} s^{-1}. The onset of the observed dramatic decrease of the Raman wavenumbers as a function of stress or strain was directly related to the existence of two yield points. The first "yield" point at relatively low applied strain/stress is thought to be associated with the plastic flow of the amorphous part. The second "yield" point at high strain/stress is possibly associated with the initiation of microcracking, which leads to the ultimate failure of the fiber. Finally, the corresponding band broadening indicated the presence of a highly nonuniform stress field acting upon the molecules of the crystalline fraction that give rise to the broad symmetric C−C and asymmetric stretching modes. A number of structural models have been reviewed in the light of the Raman data presented here.

1. Introduction

Ultrahigh molecular weight polyethylene (UHMW−PE) fibers can be produced by the process of gel-spinning followed by drawing at high temperature to very high draw ratios[1]. This technique allows for the spinning and extrusion of semidilute solutions of ultrahigh molecular weight polyethylene with average molecular weight (M_w) up to 2.4×10^{62}, whereas conventional polyethylene fibers have molecular weights in the range 10^4−10^5. The UHMW−PE fibers exhibit ultrahigh Young's moduli in the range of 100−200 GPa and very high tensile strengths of 2−5 GPa. They have also been found to have low density, good energy absorption, and chemical resistance.[1,3] These unique properties of UHMW−PE are due to their fully extended and aligned chain configuration. There is a general agreement that, structurally, these fibers consist of assemblies of smaller fibers, which, in turn, embody microfibrils of extended polymer chains.[4] In most cases a shish kebab morphology is formed, which consists of core microfibrils with nearly extended chains and a number of chain-folded platelets attached to the cores.[5]

Many structural models have been proposed to explain the relationship between the microstructure and mechanical properties of the highly oriented linear polyethylene, and two very different approaches have generally been used. According to the *fiber-reinforced model*[6] the oriented polymer consists of a reinforcing needlelike crystal phase embedded in a partially oriented amorphous phase. A completely different model assumes that the reinforcement comes from taut-tie molecules[7] and intercrystalline bridges.[8] Finally, mechanical models such as the Takayanagi model[9] recognize the two-phase nature of the semicrystalline polymers, and the mechanical behavior of an oriented fiber such as UHMW−PE is explained in terms of two separate components representing crystalline and amorphous fractions placed in either parallel−series or series−parallel configurations.[10,11]

Although the strength and stiffness of UHMW−PE fibers are exceptionally high, they are still far from the theoretical predictions. Commonly used theoretical and semiempirical values for modulus and strength along the carbon chain are about 300[12] and 35 GPa,[13] respectively. Therefore, it is of considerable scientific interest to understand the structural parameters which control the mechanical behavior and to assess what mechanisms or defects cause this deviation from the theoretical models.

Experimental techniques that can yield information concerning the relation between microscopic morphology and mechanical properties can be invaluable in understanding the behavior of these fibers. Spectroscopic methods, in particular, Raman spectroscopy, have been used extensively to study the structure and the deformation behavior of high modulus/high strength

* To whom all correspondence should be addressed at the Foundation of Research and Technology−Hellas. E-mail= c.galiotis@iceht.forth.gr.
† National Technical University of Athens.
‡ Queen Mary & Westfield College.
§ The Foundation of Research and Technology−Hellas.

S0024-9297(96)01498-2 CCC: $15.00
Published on Web 09/16/1998

fibers at the molecular level.[14−20] In highly oriented systems, an applied stress is directly translated into deformtion (bond angles and bond lengths) of the polymer backbone. Due to the anharmonicity of the atomic bonds, this brings about changes in the fiber vibrational spectra, which can be probed by either infrared or Raman spectroscopy. In general, a tensile stress causes a shift of Raman bands to lower wavenumbers whereas the reverse effect is observed in compression.[14−20] A great deal of work using micro-Raman spectroscopy has been reported in the past on polydiacetylene,[14] aramid,[15] carbon,[16] poly(*p*-phenylene benzobisthiazole),[17,18] and also polyethylene[10,11,19−24] fibers/oriented films.

In the case of PE fibers, both C−C asymmetric stretching mode B_{1g} (1060 cm^{-1}), and symmetric stretching mode A_g (1130 cm^{-1}) bands split, upon stretching, into two components,[10,11,19−22,24] which shift to lower wavenumbers but at a different rate. This has been interpreted as being due to a bimodal stress distribution of the C−C bonds of the fibers.[19−22]

Wool and Bretzlaff[23] studied ultradrawn UHMW−PE films stressed up to 0.4 GPa and reported shifts of the asymmetric C−C stretching mode (∼1059 cm^{-1}) in the range −5.7 to −11.2 cm^{-1}/GPa. For the symmetric C−C stretching mode (∼1127 cm^{-1}) a shift of −5.9 cm^{-1}/GPa for low stresses was observed.[23] Tashiro et al.[10] applied a stress up to 1.2 GPa to drawn gel PE fibers and found a shift of −6.0 cm^{-1}/GPa for the 1064 cm^{-1} band and one of 4.5 cm^{-1}/GPa for the 1130 cm^{-1} band. Prassad and Grubb[19] studied the influence of stress (up to 2.3 GPa) on the asymmetric C−C stretching mode band. The change in the peak position was linear at low stresses (−4.0 ± 0.5 cm^{-1}/GPa) and did not change at further increase of stress, but at the low-wavenumber side a tail appeared.[19] Kip et al.[20] studied the 1064 and 1130 cm^{-1} bands at room temperature and found that for fiber strains of over 1.5%, each of the C−C stretch bands split into two peaks: a narrow peak which exhibited only a small shift and a broad peak which was considerably shifted and contained 40% of the area in the band. According to Kip et al.,[20] the component of the C−C bonds which exhibits the highest shift is highly stressed, whereas the less sensitive band supports a lower stress. More recently, Wong and Young[25] reported that band splitting was evident also in the as-received fibers and that the rate of wavenumber shift for the high-load bearing "broad" band increased from about 1.5 to 7 cm^{-1}/% as the fiber modulus increased from 40 to 170 GPa.[25] The same authors[11] calculated a stress induced band shift of 0.03 cm^{-1}/GPa, which is at least 2 orders of magnitude lower than that determined experimentally by all previous authors.[19,20,23]

Wide-angle X-ray scattering has confirmed that the bimodal stress distribution exists on the crystal level.[2,20,21] Thus, it has been suggested that the fibers at the molecular level consist of two crystalline fractions with an additional small amount of a third fraction with low Young's modulus. Most X-ray experiments have been carried out at low temperatures to suppress the considerable stress relaxation of the PE fibers.[22]

All the Raman work mentioned above was conducted in as stepwise fashion due to the large exposure times required for the collection of the Raman spectra. Hence the exact rate of deformation could only be estimated by extrapolation and the Raman data could not be related to observed changes in the mechanical data. Since PE fibers exhibit large strain rate effects even at room temperature, the inability to perform real-time Raman experiments during the mechanical deformation of the PE fibers at specific strain rates, presented a very serious drawback and cast doubt on the validity of the Raman wavenumber vs stress or strain data. In this program of study, a remote laser Raman probe (ReRaM) has been built and tested[25] to allow in-situ/real-time measurements during mechanical loading of individual filaments. The new Raman system utilized flexible fiber-optic cables for laser delivery and collection and was sensitive enough to permit continuous spectra acquisition at low-to-moderate strain rates. Thus, there was no need for extrapolation to the Raman spectra of unrelaxed specimens or to conduct the Raman experiments at liquid-nitrogen temperatures. Hence, the effect of the strain rate upon the Raman vibrational spectra could be studied and related to the observed macromechanical behavior.

2. Experimental Section

2.1. Materials. A commercial UHMW−PE fiber was used for the tension and stress relaxation experiments. The fiber was supplied by Mitsui Petrochemicals Industries Ltd., under the trade name Tekmilon NA 310.

2.2. Mechanical Testing. The PE fibers were loaded on a 20kN Hounsfield screw-driven tensile tester machine. The specimens were 50 mm in gauge length and were tested in tension at room temperature at different strain rates of 1.67×10^{-4}, 3.33×10^{-4}, 5.00×10^{-4}, 8.33×10^{-4} and 1.67×10^{-3} s^{-1}. The individual monofilaments were mounted across a hole on a paper card. At each end, the fiber was twisted around a bar and was stacked in the card using the HY 5161/CY 219 (Ciba Geigy) epoxy resin system. The curing was carried out at room temperature. The monofilament had to be strongly fixed on the card, to avoid fiber slipping during the experiment. The card was mounted between the testing grips of the mechanical tested and then the card edges were cut.

2.3. Raman Spectroscopy. The remote laser Raman microprobe (ReRaM) which was used in this work is shown in Figure 1.[25] The input laser light of the 514.5 nm line of an argon ion laser was directed to the objective of a conventional microscope via a single-mode fiber-optic and then was focused onto the specimen which undergoes mechanical deformation.[25] A 50× long working distance objective of N.A. = 0.55 was employed for the focusing the beam to the fibers. The laser beam was polarized parallel to the fiber axis at a constant laser power at specimen of 7 mW. Finally, the 180° scattered light was collected by another fiber optic and was, then, directed to a single monochromator for analysis and Raman detection. Additional details of the experimental Raman system are given in ref 25.

It was found that no visible degradation in the fiber was observed up to 20 mW of laser power. This is not surprising since, as mentioned in the review article by Porter et al.,[26] the thermal conductivity of UHMW polyethylene fibers in the fiber direction at room temperature is of the same order of magnitude as that of copper and, therefore, the heat generated by the incident laser power can be easily dissipated. Hence, a very short exposure time of 2 s at 7 mW laser power was

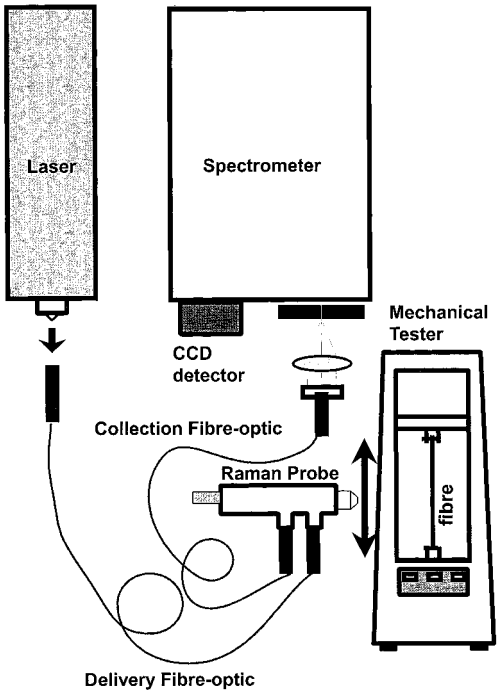

Figure 1. Remote laser Raman spectroscopy set up employed for the on-line stress measurements on the UHMW polyethylene fibers.

employed for the acquisition of each Raman spectrum during loading of the filaments at the specified strain rates. On the basis of this analysis, further improvements in the Raman detection time are still possible and open the way for on-line measurements at even higher strain rates. It is worth reporting that the detection times that had been employed in the past by other workers were much higher, in the range of 50[24] to 180 s,[21,22] and therefore, stress relaxation effects could not be avoided during recording of the Raman spectra. The reported significant improvement in the detection time was also due to the efficiency of the optical assembly and the use of fast charge-coupled devices (CCD) for light detection.[25]

Table 1. Relative Positions and Bandwidths of the C−C Asymmetric and Symmetric Stretch Bands (All Bands Fitted with Gaussian Curves)

band	position/ cm^{-1}	fwhm/ cm^{-1}	χ^2
C−C asymmetric stretch (B_{1g})	1059	4.4 ± 0.20	0.11 ± 0.02
broad band			
narrow band	1060	2.2 ± 0.22	
C−C symmetric stretch (A_g)	1128	10.6 ± 0.20	1.3 ± 0.5
broad band			
narrow band	1130	4.2 ± 0.05	

3. Results

A selection of Raman spectra, taken from a PE monofilament at different applied strains at room temperature, are presented in Figure 2. As can be seen from the raw data (Figure 2), the level of fluorescence is negligible and the background appears linear, and hence, all spectra from 1000 to 1170 cm^{-1} were fitted with a linear background. Both symmetric (1130 cm^{-1}) and asymmetric (1060 cm^{-1}) C−C stretching mode Raman bands of the as-received fiber were deconvoluted as a sum of one "broad" and one "narrow" Gaussian curves (Table 1). This pointed to the existence of Raman band splitting prior to application of stress, as found also by Wong and Young.[24] The intensity of the asymmetric C−C stretching band of the Tekmilon fiber was relatively lower than that of the symmetric band. All bands within the 1000−1170 cm^{-1} spectral window were found to shift to lower wavenumbers and to broaden considerably with applied stress or strain.

The tensile stress−strain curves of polyethylene monofilaments for two extreme values of strain rates are presented in Figure 3. The stress−strain relationships were essentially nonlinear; the strain rate did not appear to affect significantly the initial values of tensile modulus (up to 5% strain), but it did have some effect upon the ultimate tensile stress of the fiber (Figure 3, Table 2). The secant modulus (up to 0.5%) and the tensile strength of the fiber at a strain rate of 1.67 × 10^{-3} s^{-1} were measured to be 50 and 2.02 GPa, respectively (Table 2).

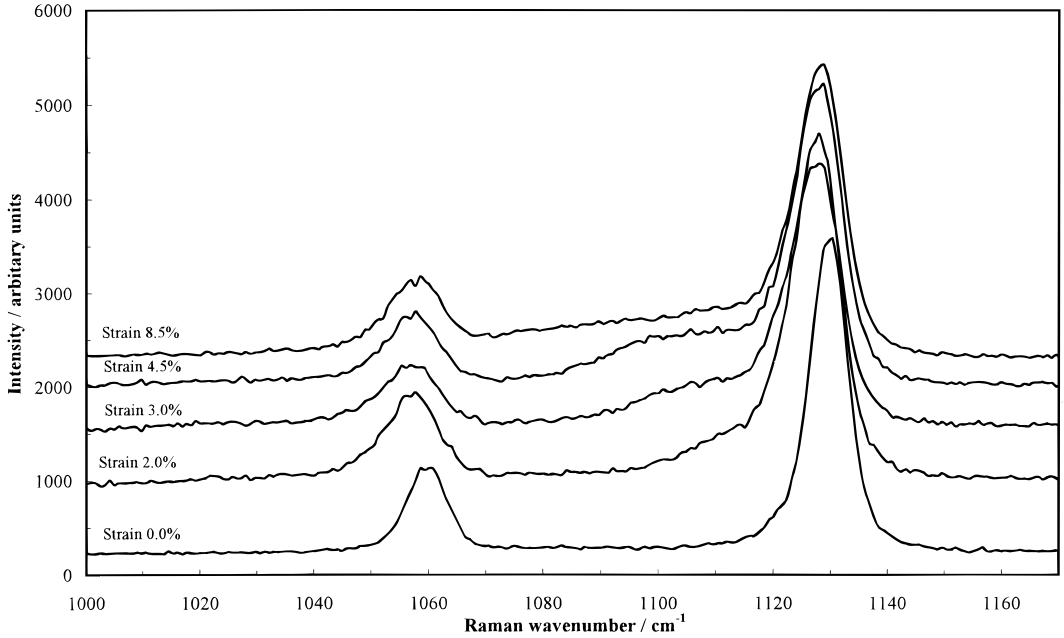

Figure 2. Raman spectra of PE monofilaments during tension at room temperature, as a function of strain.

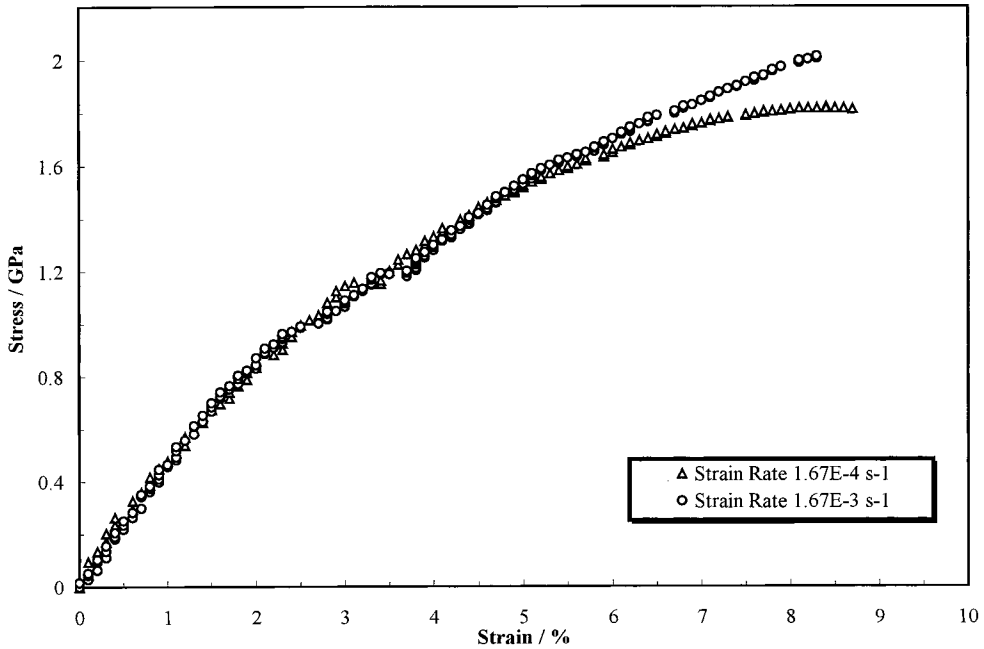

Figure 3. Typical tensile stress−strain curves of PE monofilaments at room temperature and at two different strain rates.

Table 2. Effect of Strain Rate on Tensile Strength of PE Monofilaments for a Gauge Length of 50 mm

strain rate/s^{-1}	tensile strength/GPa	strain at the breaking point/%
1.67×10^{-4}	1.82	8.4
3.33×10^{-4}	1.87	9.2
5.00×10^{-4}	2.01	9.6
8.33×10^{-4}	2.00	8.9
1.67×10^{-3}	2.02	8.3

Electron micrographs of fracture surfaces of specimens tested at a strain rate of 1.67×10^{-3} s^{-1} revealed significant fibrillation upon fracture (Figure 4). Kink bands were also observed on the surface of the fractured fiber possibly due to fiber recoiling and subsequent compression failure. Such kink bands in polyethylene can cause stress concentration and microcracking, which lead to fiber fibrillation at tensile failure.[28,29]

The Raman wavenumber shift and the full width at half-maximum (fwhm) of all bands as a function of applied strain and stress at a representative strain rate of 1.67×10^{-4} s^{-1} are presented in Figures 5−12 and Tables 3−6. The effect of strain rate upon the observed wavenumber shift is also given in Tables 3−6 for both the symmetric (Tables 3a,b and 4a−d) and asymmetric (Tables 5a,b and 6a,b) C−C stretching modes.

The Raman wavenumber of the symmetric "narrow" C−C stretching band shown in Figure 5, decreased with strain up to a value of 1.3% and then formed a plateau followed by a gradual increase up to fracture (Figure 5). The shifts of the Raman wavenumber as a function of the strain rate, assuming a linear trend up to the inversion point, are given in Table 3a. As shown, an average value on the order of -2 cm^{-1}/% was obtained from all five strain rates. On the other hand, the fwhm increased by 2 cm^{-1} up to 3% strain and then formed a plateau. With regard to the stress sensitivity of the same band shown in Figure 6, the Raman wavenumber decreased linearly up to a value of 0.6 GPa and then formed a plateau up to 1.1 GPa of stress, followed by a gradual increase up to fracture. The average slope of the least-squares-fitted line up to 0.6 GPa was found to be -4.6 cm^{-1}/GPa for all five strain rates (Table 3b). Again, an inverse relationship between Raman wave-

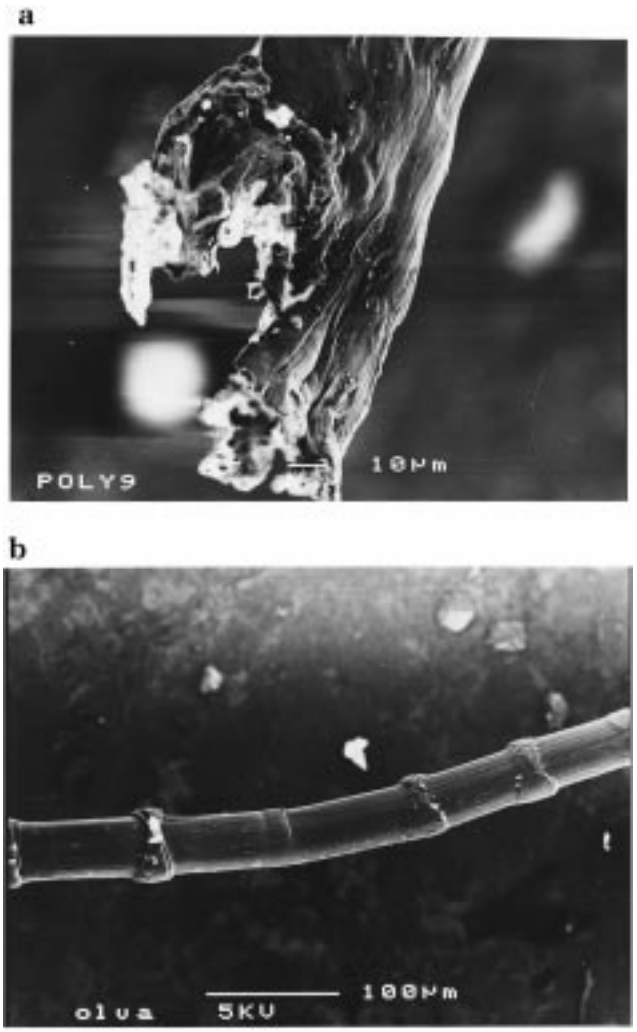

Figure 4. SEM photomicrographs after failure at tension of PE monofilament using a train rate of 1.67×10^{-4} s^{-1}: (a) at the fracture point and (b) along the surface of the fractured fiber.

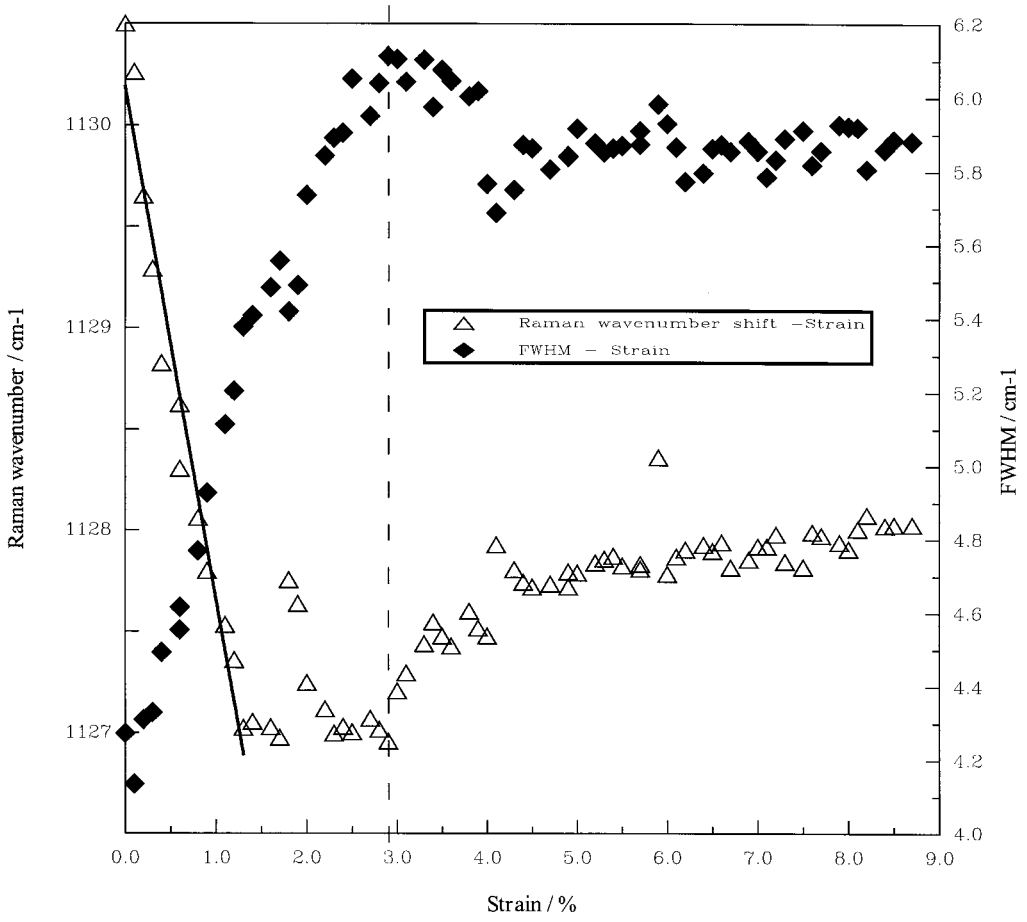

Figure 5. Raman wavenumber of the "narrow" symmetric C−C stretching mode band and full bandwidth at half-maximum (fwhm) as a function of strain at room temperature and at a strain rate of 1.67×10^{-4} s^{-1}. The solid line represents a least-squares fit to the Raman wavenumber vs strain data points up to 1.3% strain.

number shift and fwhm was obtained; the fwhm increased with stress by 2.7 cm^{-1} up to approximately 1.1 GPa and then decreased slightly.

In Figure 7 the Raman wavenumber and the fwhm are plotted as a function of applied strain for the "broad" symmetric C−C stretching band. The relationship between Raman wavenumber and applied strain was divided in three different regions: In region I, up to 1.2% strain, a linear relationship was assumed of a corresponding least-squares-fitted slope of −3.0 cm^{-1}/% (Table 4a). Region II covered the 1.3−7.0% range of strains and was fitted with a second degree polynomial, the first derivative, b, of which was calculated to be −6.1 cm^{-1}/% at 1.3% strain (Table 4b). Finally, in region III the Raman wavenumber was found to increase again by approximately 1 cm^{-1} (Figure 7). The value of strain required for the transition from region II to region III was found to be highly dependent upon the strain rate (Table 4b). The fwhm for the "broad" symmetric C−C stretching band remained constant up to a strain of approximately 1.3% (region I) and then increased dramatically by approximately 20 cm^{-1} up to about 7% of applied strain. As can be seen in Figure 7, for the strain regime of 1.3 to 7% an inverse relationship between the Raman wavenumber shift and fwhm was obtained. It is interesting to note that the observed slight increase of the Raman wavenumber for strains higher than 7% was also mirrored by a corresponding decrease of the fwhm.

In Figure 8 the Raman wavenumber and the fwhm are plotted as a function of applied stress for the "broad" symmetric C−C stretching band. Again the overall relationship was divided into three distinct regions: In region I, up to approximately 0.6 GPa stress, a linear relationship was assumed of a corresponding least-squares-fitted slope of −6.7 cm^{-1}/GPa (Table 4c). Region II covered the 0.6−1.7 GPa range of stresses and could be fitted with a second least-squares-fitted line, which had a slope of −14.6 cm^{-1}/GPa (Table 4d). Finally, in region III, the Raman wavenumber increased again by approximately 2 cm^{-1} (Figure 8). The fwhm of the "broad" symmetric C−C stretching band remained constant up to about 0.6 GPa and then increased by about 20 cm^{-1} up to a stress of about 1.7 GPa. As in all previous cases (Figures 6 and 7), for stresses higher than 0.6 GPa an inverse relationship between Raman wavenumber shift and fwhm was again obtained (Figure 8). It is interesting to note here that no systematic trend between the Raman wavenumber and strain or stress was observed for the "broad" symmetric C−C stretching mode (Table 4b,c).

The Raman wavenumber of the asymmetric "narrow" C−C stretching band shown in Figure 9, decreased linearly with strain up to a value of 1.3% and then formed a plateau (Table 5a). The slope of the least-squares-fitted line up to 1.1% strain for the strain rate of 1.67×10^{-4} s^{-1} was found to be −2.2 cm^{-1}/%. Generally the magnitude of the strain sensitivity decreased with strain rate but the level of uncertainty

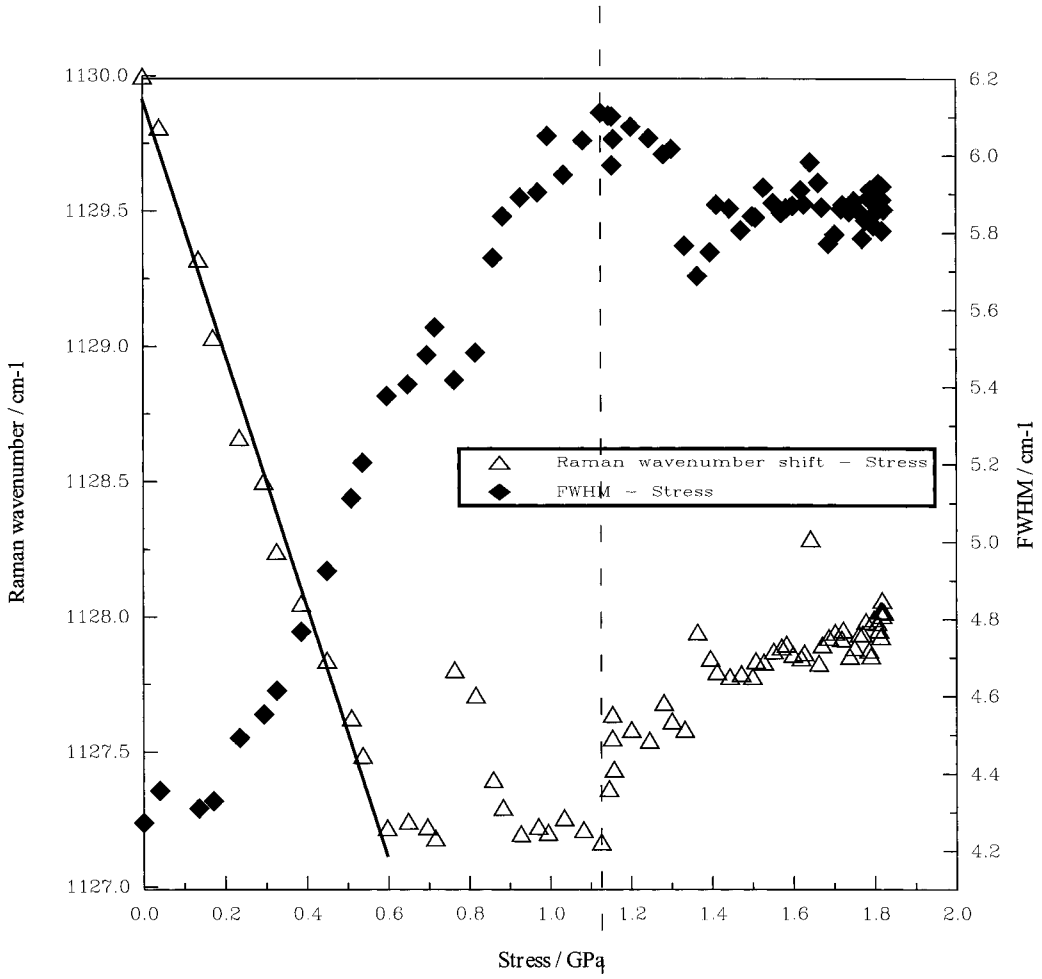

Figure 6. Raman wavenumber of the "narrow" symmetric C−C stretching mode band and full bandwidth at half-maximum (fwhm) as a function of stress at room temperature and at a strain rate of 1.67×10^{-4} s^{-1}. The solid line represents a least-squares fit to the Raman wavenumber vs stress data points up to an applied stress of 0.6 GPa.

increased. The corresponding fwhm was found to increase by 2.5 cm^{-1} up to 3% strain, formed a plateau up to 5%, and then decreased again. In Figure 10, the stress sensitivity of the same band is shown for the 1.67×10^{-4} s^{-1} strain rate. As seen, the Raman wavenumber decreased linearly up to a value of 0.5 GPa and then formed a plateau. The average slope of the least-squares-fitted line up to 0.6 GPa was found to be −3.9 cm^{-1}/GPa for all five strain rates (Table 5b). Again, an inverse relationship between the Raman wavenumber and fwhm was obtained; the fwhm increased with stress by 2.5 cm^{-1} up to approximately1.1 GPa and then decreased by 1.4 cm^{-1} up to fracture (Figure 10). In general, the observed trends for the symmetric (Figures 5 and 6) and the asymmetric (Figures 9 and 10) "narrow" C−C stretching modes were very closely related.

In Figure 11 the Raman wavenumber and the fwhm are plotted as a function of applied strain for the "broad" asymmetric C−C stretching band. As can be seen, the experimental scatter increased dramatically at high applied strains. This was due to the very weak intensity of the asymmetric C−C stretching band and the corresponding difficulty in peak fitting particularly at high strains where the peak "smears out" considerably (Figure 11). A linear relationship could only be assumed up to 1.1% of a corresponding least-squares-fitted slope of −4.6 cm^{-1}/% (Table 6a). This value decreased somewhat with strain rate although there was no systematic trend to report (Table 6a). The results for strain rates higher than 3.33×10^{-4} s^{-1} exhibited an unacceptable degree of scatter and could not be reported. The fwhm for the "broad" asymmetric C−C stretching band increased very slightly up to 1.1% (linear region) and then increased exponentially by approximately 20 cm^{-1} up to about 6% of applied strain.

In Figure 12 the Raman wavenumber and the fwhm are plotted as a function of applied stress for the "broad" symmetric C−C stretching band. The overall relationship could also be divided in three regions: In region I, up to 0.5 GPa stress, a linear relationship was assumed of a corresponding least-squares-fitted slope of −9.8 cm^{-1}/GPa (Table 6b). Region II covered the 0.5−1.5 GPa range of stresses and corresponded to a region that exhibited a pronounced decrease of the Raman wavenumber (Table 6c) albeit a very high experimental scatter. Finally, in region III (>1.5 GPa) the Raman wavenumber was found to increase again. The fwhm of the "broad" symmetric C−C stretching band, remained approximately constant up to about 0.5 GPa (linear region) and then increased by about 20 cm^{-1} up to a stress of about 1.5 GPa. As previously (Figure 8), for stresses higher than 0.5−0.6 GPa, an inverse relationship between Raman wavenumber shift and fwhm was obtained. Only results up to a strain rate of 3.33×10^{-3} s^{-1} could be reported due to the unacceptable degree of data scatter observed for higher strain rates for the weak asymmetric C−C stretching mode.

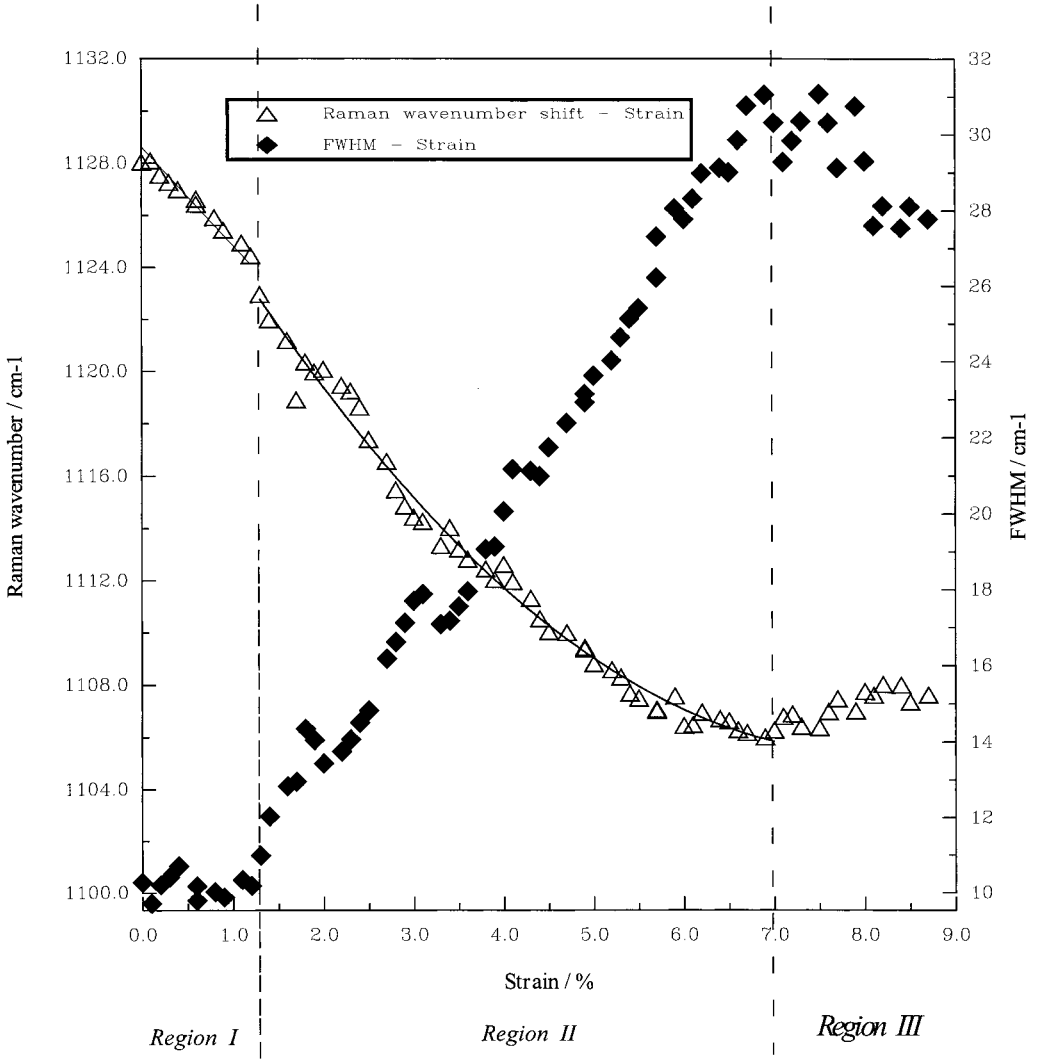

Figure 7. Raman wavenumber of the "broad" symmetric C−C stretching mode band and full bandwidth at half-maximum (fwhm) as a function of strain at room temperature and at a strain rate of 1.67×10^{-4} s^{-1}. The two solid lines represent (a) a least-squares fit to the Raman wavenumber vs strain data points up to 1.3% strain and (b) a second degree polynomial fit to the Raman wavenumber vs strain data points within the 1.3−1.7% range of strain values.

4. Discussion

4.1. Effect of Strain Rate. As is well-known, polyethylene fibers, unlike other high performance fibers, are highly viscoelastic,[2] and therefore, real-time measurements are required in order to monitor actual molecular processes by spectroscopic means during mechanical deformation of these fibers. The results presented here are a first attempt to relate Raman spectroscopic data to stress or strain without the need for extrapolation to zero strain rates or for cooling the specimens to low temperatures. However, the exposure time of 2 s employed here, even though it is a great improvement on previous work,[21,22,16] still does not allow measurements at relatively high strain rates. Hence, only low to moderate strain rates (10^{-4}−10^{-3} s^{-1}) could be applied and the results showed that the Raman wavenumber shift of both the asymmetric and the symmetric ("narrow" plus "broad) bands per applied stress/strain was not found to be strongly affected within experimental error. The only clear increase of the absolute value of the wavenumber shift per stress was observed in the steep second part of the Raman wavenumber vs applied stress relationship of the "broad" symmetric stretching band (Table 4d, Figure 8). The corresponding results of the "broad" asymmetric stretching band exhibited a great deal of scatter and no firm conclusion could be drawn (Figure 12). The onset of the Raman wavenumber plateau, as well as, the maximum value of the wavenumber shift were found to increase with increasing strain rate.

4.2. Failure Mechanisms/Yield Behavior. The application of the laser Raman spectroscopy to PE fibers has led to the identification of two types of crystalline molecules or, more appropriately, crystalline environments as indicated, for example, by the existence of the "narrow" and "broad" bands of the symmetric C−C stretching mode of the polyethylene crystalline structure. To get a global view of the changes taking place at the molecular level, it is worth summarizing the results obtained at a specific strain rate (Figures 5−12).

The first important observation was that the Raman wavenumber of both the "narrow" symmetric and asymmetric C−C stretching modes decreased linearly up to 1.1−1.3% of strain (Figures 5 and 9) or 0.5−0.6 GPa of applied stress (Figures 6 and 10). Beyond that level of strain/stress, the deconvoluted Raman wavenumber of the both C−C stretching bands formed a plateau up to 3% strain (Figures 5 and 9) or 1.1 GPa of stress (Figures

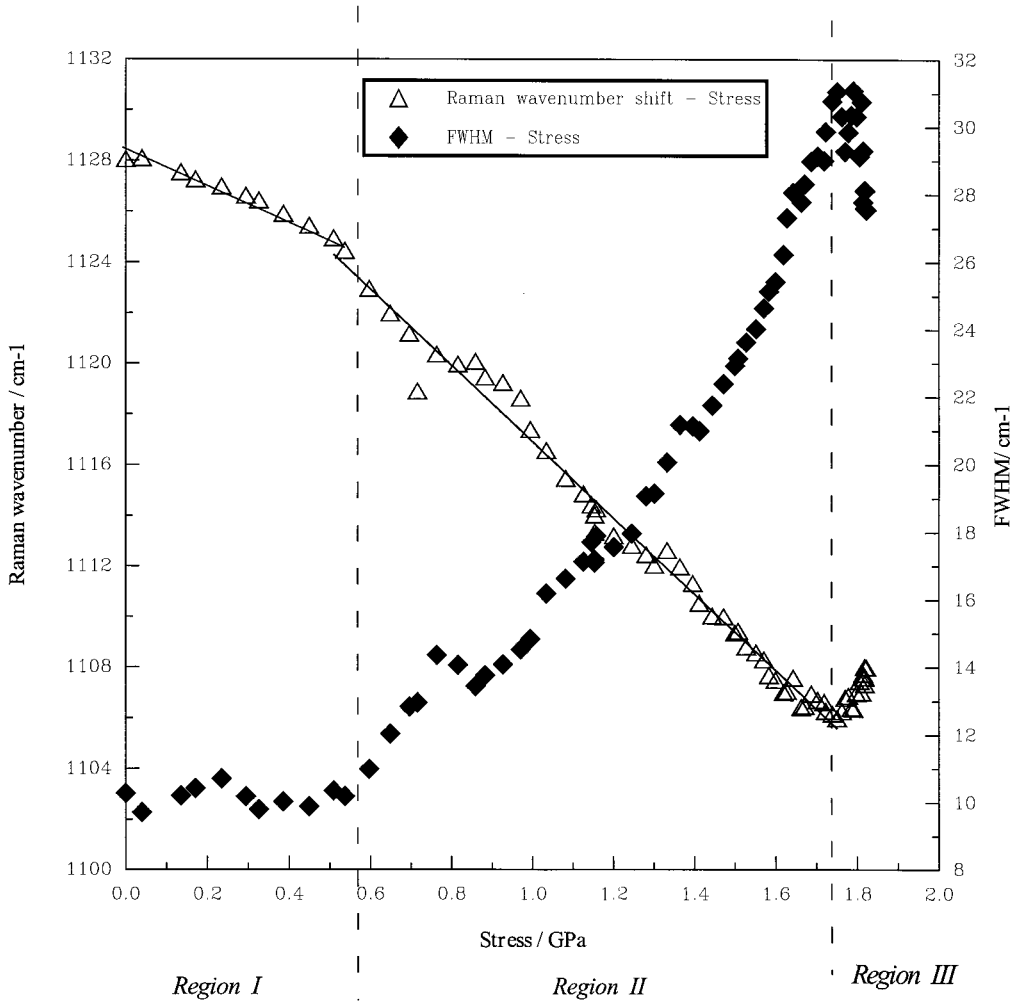

Figure 8. Raman wavenumber of the "broad" symmetric C−C stretching mode band and full bandwidth at half-maximum (fwhm) as a function of stress at room temperature and at a strain rate of 1.67×10^{-4} s^{-1}. The two solid lines represent least-squares fits to the Raman wavenumber vs stress data points within the 0−0.6 and 0.6−1.7 GPa ranges of values, respectively.

6 and 10), followed by a gradual relaxation of the Raman wavenumber to higher values. The corresponding bandwidth (fwhm) of both bands increased almost linearly up to 3% strain (Figures 5 and 9) or 1.1 GPa of stress (Figures 6 and 10). It is worth mentioning again that the results for the "narrow" asymmetric band exhibited a great deal of scatter due to the low intensity of that band for the Tekmilon fibers and the resulting difficulties in band fitting and deconvolution.

The second observation, was that the Raman wavenumber of the "broad" symmetric C−C stretching band as a function of applied strain and stress, shown in Figures 7 and 8, respectively, exhibited two distinct types of behavior:

(a) Up to 1.2% strain (Figure 7) or 0.6 GPa (Figure 8) of stress there was a linear decrease of the Raman wavenumber of about -3 cm^{-1}/% (Table 4a) and -7 cm^{-1}/GPa (Table 4c), respectively.

(b) Within the 1.2−7% (Figure 7) and 0.6−1.7 GPa (Figure 8) range of strains and stresses, respectively, the rate of change of the Raman wavenumber almost doubled. The Raman wavenumber vs strain data have been fitted by a second degree polynomial (Table 4b) of coefficient $b = -6$ cm^{-1}/%, whereas the corresponding data per stress have been fitted with a straight line of slope of approximately -15 cm^{-1}/GPa (Table 4c).

The corresponding data of the "broad" asymmetric band exhibited again a great deal of scatter for strains and stresses higher than 1.1% (Table 6a, Figure 11) and 0.5 GPa (Table 6b, Figure 12), respectively. However, the rate of change of the fwhm shown in Figures 11 and 12 was clearly similar to that of the "broad" symmetric band (Figures 7 and 8).

The Raman spectroscopic data allow an evaluation of the critical points of the stress/strain behavior of the UHMW−PE fibers. First of all the crystalline molecules which give rise to the "narrow" bands of both symmetric and asymmetric modes cannot be loaded beyond 1.1−1.3% strain or 0.5−0.6 GPa stress. This is indicated by the formation of the plateau of the Raman wavenumber vs strain/stress data and the subsequent relaxation of the Raman wavenumber toward higher values (Figures 5, 6, 9, and 10). The fwhm increased moderately by approximately 2 cm^{-1} up to 3%/1.2 GPa, at which point relaxation of the Raman wavenumber was observed. The formation of a plateau of the Raman wavenumber vs strain/stress data beyond 1.1−1.3% strain or 0.5−0.6 GPa stress is a clear manifestation of the presence of a yield point. Since the PE crystal can be deformed up to much higher values of strain/stress, then it follows that the environment through which the applied stress is transferred to the crystal, has in fact yielded. Furthermore, the fact that the stresses are locked in the crystal up to much higher deformations indicates that, at that stress value, plastic flow rather than microcracking is initiated. The only structural

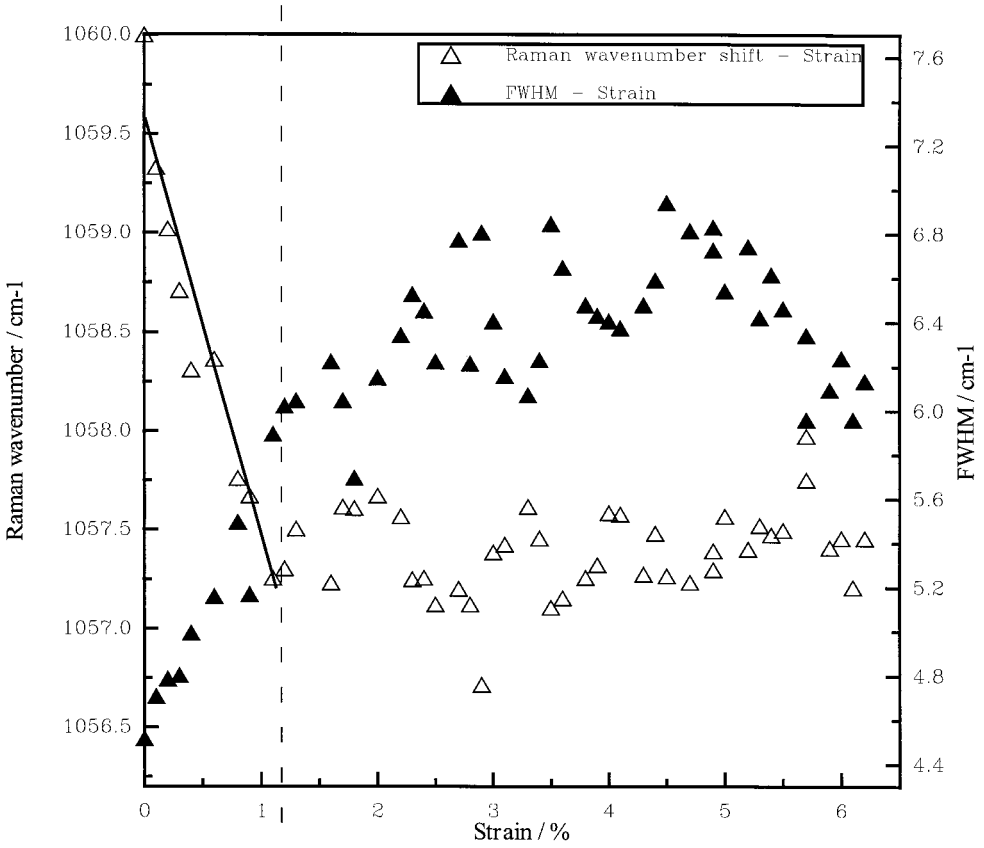

Figure 9. Raman wavenumber of the "narrow" asymmetric C−C stretching mode band and full bandwidth at half-maximum (fwhm) as a function of strain at room temperature and at a strain rate of 1.67×10^{-4} s^{-1}. The solid line represents a least-squares-fit to the Raman wavenumber vs strain data points up to 1.1% strain.

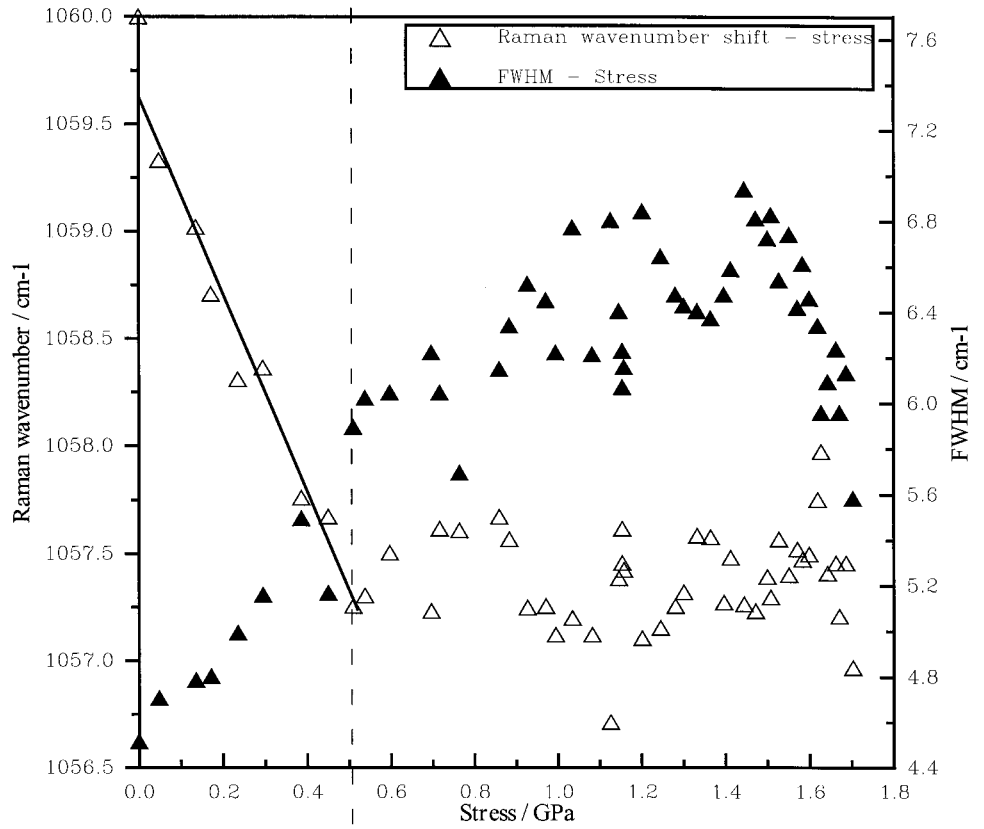

Figure 10. Raman wavenumber of the "narrow" asymmetric C−C stretching mode band and full bandwidth at half-maximum (fwhm) as a function of stress at room temperature and at a strain rate of 1.67×10^{-4} s^{-1}. The solid line represents a least-squares fit to the Raman wavenumber vs stress data points up to an applied stress of 0.5 GPa.

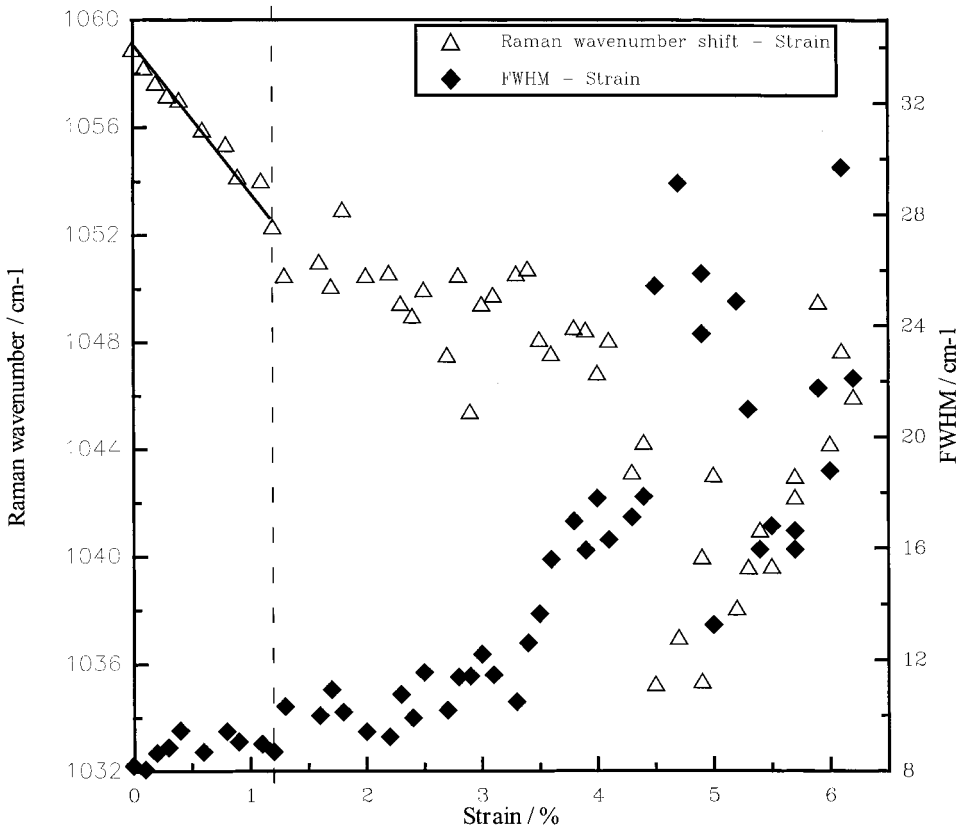

Figure 11. Raman wavenumber of the "broad" asymmetric C−C stretching mode band and full bandwidth at half-maximum (fwhm) as a function of strain at room temperature and at a strain rate of 1.67×10^{-4} s^{-1}. The two solid lines represent a least-squares fit to the Raman wavenumber vs strain data points up to 1.7% strain.

element that can account for this type of behavior is shown in Figure 13; the crystal is thought to be linked in series with highly oriented amorphous matter which has a strain−rate-dependent yield point.

The crystalline molecules that give rise to the "broad" C−C stretching modes are loaded up to the first yield point (1.1−1.3% strain or 0.5−0.6 GPa stress) at strain and stress dependent wavenumber shifts (Tables 4a,b and 6a,b), which are 1.5−2 times higher than the corresponding values obtained from the "narrow" C−C stretching bands (Tables 3a,b and 5a,b). At that point, however, the rate of shift increases considerably, and as clearly shown in the case of the symmetric mode, a second yield point is observed just prior to fiber fracture at 7% strain or 1.7 GPa stress (Figures 7 and 8). The fwhm, which is almost constant up to the first critical point (1.1−1.3% strain or 0.5−0.6 GPa stress), exhibits an overall increase of approximately 20 cm^{-1} up to the second yield point. The dramatic increase of the rate of wavenumber shift beyond the first yield point can only be due to a shear-activated stress transfer mechanism. The strongest evidence for such a mechanism emerges from the dramatic increase of the bandwidth found in this work. Indeed, the "shear−lag" type of stress transfer[30] would require a broad distribution of stresses along the crystalline fibril building from the ends and reaching a maximum at mid-length. The overall stress differential is expected to increase with applied stress, and that explains the observed relationship between fwhm and applied strain and stress of Figures 7 and 8, respectively. The structural element that can account for this type of behavior is shown also in Figure 13. The crystalline fibril is thought to be surrounded by the "matrix" material forming an equal-strain composite element. As a result of the strong interfacial forces binding the two materials together, the plastic flow (strain) of the amorphous matrix will generate a localized shear field. If we assume that the element is bound and there is enough "matrix" material around the crystal, then the two bodies ("matrix" plus crystal) will have to be strained by the same amount and, therefore, the high modulus material (crystal) will be the main bearer of the applied normal stresses.

On the basis of the above, it is interesting to examine how the two elements are now linked together in the fiber. First of all it is interesting to review other structural models which have been proposed in order to provide possible explanations for the Raman data. The model proposed by Prevorsek[2] incorporates most of the ideas presented here; however, the presence of a continuous inter-amorphous phase is questionable. If such a phase were present, then, at stresses higher than its yield point, all crystals would have had to be subjected to a shear−lag type of stress buildup. This would have given rise to only one, extremely "broad", Raman peak, but, it would not have yielded a weak "broad" peak adjacent to an intense "narrow" band as observed in all Raman spectra regardless of fiber type. The Takayanagi parallel-series model[9] employed by Tashiro et al.[10] and by Wong and Young,[11] captures the essence of the morphology of the fiber but it fails to predict the stress-transfer at higher applied loads. This is because the Takayanagi model is by definition a 1-D model and, therefore, is unable to incorporate shear displacements within the structure. It is interesting to note here that Wong and Young[11] have assumed that the stress-sensitivity of the Raman wavenumber, k (eq 1 of ref 11), is the same for both elements of the model.

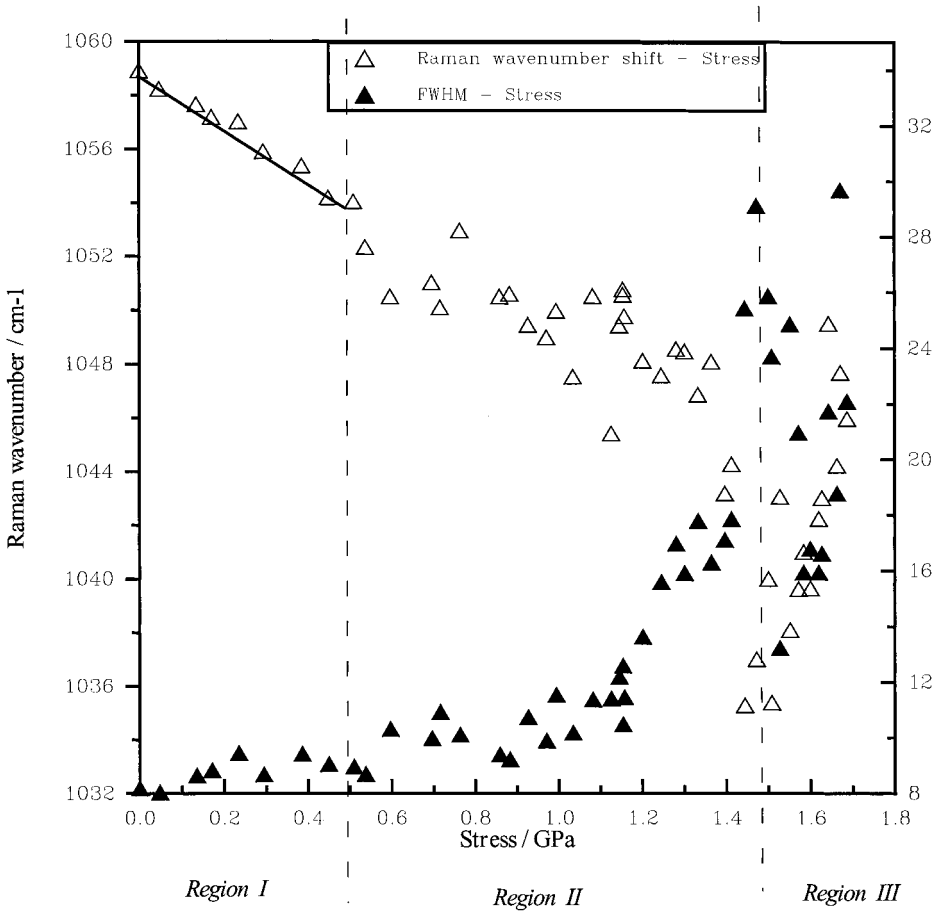

Figure 12. Raman wavenumber of the "broad" asymmetric C−C stretching mode band and full bandwidth at half-maximum (fwhm) as a function of stress at room temperature and at a strain rate of 1.67×10^{-4} s^{-1}. The two solid lines represent a least-squares fit to the Raman wavenumber vs stress data points within the 0−0.5 GPa range of values.

Table 3. Dependence of the Narrow Symmetric C−C Stretching Mode Band upon Applied Strain for the Initial Part of the Curve for Which a Linear Fit Was Applied (Corresponding Statistical Parameters Also Listed)

(a) "Narrow" Symmetric C−C Stretching Mode Band vs Applied Strain

strain rate/s^{-1}	slope/ (cm %)$^{-1}$	range/ %	std error/ (cm %)$^{-1}$	intercept/ cm^{-1}	R^2
1.67×10^{-4}	−2.0	0−1.3	0.1	1129.7	0.959
3.33×10^{-4}	−1.9	0−1.3	0.1	1130.2	0.989
5.00×10^{-4}	−2.2	0−1.2	0.1	1130.1	0.985
8.33×10^{-4}	−2.1	0−1.5	0.2	1129.8	0.961
1.67×10^{-3}	−2.1	0−1.2	0.05	1130.8	0.999

(b) "Narrow" Symmetric C−C Stretching Mode Band vs Applied Stress

strain rate/s^{-1}	slope/ (cm GPa)$^{-1}$	range/ GPa	standard error/ (cm GPa)$^{-1}$	intercept/ cm^{-1}	R^2
1.67×10^{-4}	−4.6	0−0.6	0.2	1129.9	0.988
3.33×10^{-4}	−4.4	0−0.7	0.2	1130.3	0.981
5.00×10^{-4}	−4.5	0−0.6	0.2	1130.1	0.989
8.33×10^{-4}	−4.8	0−0.6	0.4	1129.9	0.992
1.67×10^{-3}	−4.6	0−0.8	0.1	1130.0	0.999

Such an assumption is only valid for paracrystalline fibers such as the aramids, which obey the equal-stress model,[13] but it cannot be applied to UHMW−PE. Thus, it is not surprising that their calculated vales of k of 0.03 cm^{-1}/GPa is at least 2 orders of magnitude lower than values derived experimentally by all previous workers.[10,19,23]

The most appropriate structural model for the Raman data presented here requires the presence of a highly oriented but discontinuous amorphous phase that can be packed both in-parallel and in-series with the crystalline material. The earlier model by Gibson et al.[8]—reviewed also in ref 27—can be employed to account for the results obtained by Raman spectroscopy. As can be seen in Figure 13, this model is basically a Takayanagi model, which has been modified to allow shear displacements around the crystalline "bridges".[27] However, the fibrillar structure of UHMW−PE requires that the crystalline blocks are fibrillar in nature, while some discontinuous interamorphous material may still be present (Figure 13). As can be seen in Figure 13, the crystalline material is in-parallel with the highly strained (drawn) amorphous "matrix" and, therefore, will be have to be in tension, hence, the shift of the Raman wavenumbers of a crystalline "bridge" to lower values in the as-received fibers.[25] The lower relative intensity of the "broad" C−C stretching band (∼35% of total) for the Tekmilon fibers reflects the amount of crystalline material which is in-parallel with the amorphous phase (Figure 13). Finally, the increase of the intensity of this band with stress observed by some authors[20,24] maybe due to either stress-induced crystallization or to an effective increase of the length of the crystalline "bridges" as the adjacent crystalline material relaxes for any stresses higher than the first yield point (Figures 7 and 8).

5. Conclusions

Real-time Raman measurements were conducted on ultrahigh-molecular-weight polyethylene monofilaments

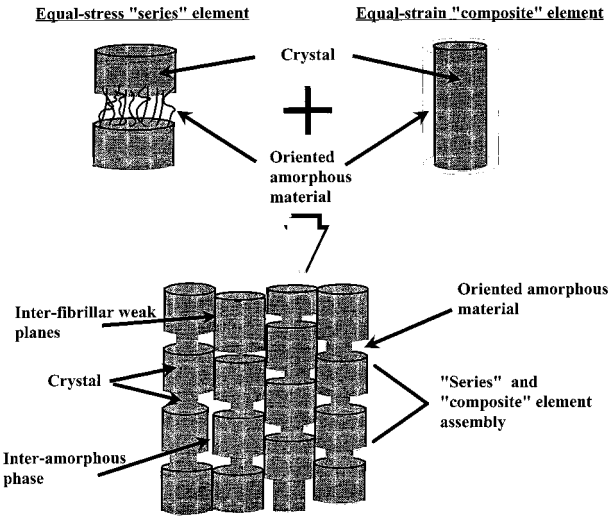

Figure 13. Proposed structural models based on the results obtained in this work.

Table 4. Dependence of the "Broad" Symmetric C−C Stretching Mode Band upon Applied Strain or Stress for the Initial Part of the Curve for Which a Linear Fit Was Applied or the Second Part of the Curve for Which a Second Degree polynomial Fit Was Applied (Corresponding Statistical Parameters Also Listed)

(a) "Broad" symmetric C−C Stretching Mode Band vs Applied Strain

strain rate/s^{-1}	slope/ $(cm\ \%)^{-1}$	range/ %	std error/ $(cm\ \%)^{-1}$	intercept/ cm^{-1}	R^2
		First Range			
1.67×10^{-4}	−3.0	0−1.2	0.1	1128.2	0.990
3.33×10^{-4}	−2.4	0−1.3	0.3	1129.0	0.928
5.00×10^{-4}	−2.7	0−1.2	0.2	1128.7	0.971
8.33×10^{-4}	−2.9	0−1.5	0.2	1128.3	0.989
1.67×10^{-3}	−2.1	0−1.2	0.05	1128.5	0.999

(b) "Broad" Symmetric C−C Stretching Mode Band vs Applied Strain

strain rate/s^{-1}	range/ %	a/cm^{-1} $(\%)^{-2}$	$b/$ $(cm\ \%)^{-1}$	c/cm^{-1}	R^2
		Second Range: Second Degree Polynomial Fit of the Form $ax^2 + bx + c$			
1.67×10^{-4}	1.3−7.0	0.4	−6.1	1130.1	0.989
3.33×10^{-4}	1.3−8.0	0.2	−5.5	1133.1	0.991
5.00×10^{-4}	1.2−7.5	0.3	−6.6	1133.5	0.989
8.33×10^{-4}	1.5−10.0	0.2	−5.0	1131.5	0.980
1.67×10^{-3}	1.2−8.3	0.2	−5.3	1132.4	0.987

(c) "Broad" Symmetric C−C Stretching Mode Band vs Applied Stress

strain rate/s^{-1}	slope/ $(cm\ GPa)^{-1}$	range/ GPa	std error/ $(cm\ GPa)^{-1}$	intercept/ cm^{-1}	R^2
		First Range			
1.67×10^{-4}	−6.7	0−0.6	0.2	1128.4	0.975
3.33×10^{-4}	−7.3	0−0.8	0.6	1129.6	0.936
5.00×10^{-4}	−8.1	0−1.0	0.6	1128.3	0.953
8.33×10^{-4}	−7.2	0−0.9	0.3	1128.6	0.992
1.67×10^{-3}	−6.7	0−0.8	1.1	1128.7	0.944

(d) "Broad" Symmetric C−C Stretching Mode Band vs Applied Stress

strain rate/s^{-1}	slope/ $(cm\ GPa)^{-1}$	range/ GPa	std error/ $(cm\ GPa)^{-1}$	intercept/ cm^{-1}	R^2
		Second Range			
1.67×10^{-4}	−14.6	0.6−1.7	0.6	1131.8	0.953
3.33×10^{-4}	−19.3	0.8−1.9	0.4	1139.2	0.983
5.00×10^{-4}	−19.4	1.0−2.0	0.5	1139.0	0.988
8.33×10^{-4}	−18.4	1.0−1.9	1.1	1137.5	0.964
1.67×10^{-3}	−18.0	1.1−2.0	0.9	1138.2	0.987

produced by Mitsui Petrochemicals. The best fits to the Raman data were obtained by fitting a linear background, one Gaussian curve to the asymmetric mode and two Gaussian curves to the symmetric C−C stretching modes. The stress and strain dependence of the Raman wavenumbers of both the symmetric and asymmetric C−C stretching mode bands were examined as a function of strain rate at room temperature. The Raman band shift for the asymmetric and symmetric C−C stretching modes per stress or strain was found to be only marginally affected for the 10^{-4}−10^{-3} s^{-1} range of strain rates.

The Raman wavenumber of the "narrow" symmetric and asymmetric C−C stretching modes decreases linearly up to 1.1−1.3% strain or 0.5−0.6 GPa stress and then forms a plateau up to 3% strain or 1.2 GPa stress, depending on strain rate, followed by a gradual relaxation of the Raman wavenumber to higher values. The Raman wavenumber of the "broad" symmetric C−C stretching band as a function of applied strain and stress decreases linearly up to 1.1−1.3% strain or 0.5−

Table 5. Dependence of the "Narrow" Asymmetric C−C Stretching Mode Band upon Applied Strain or Stress, Where the Range within Which a Linear Fit Was Applied and the Corresponding Statistical Parameters Are Listed

(a) Asymmetric C−C Stretching Mode Band vs Applied Strain

strain rate/s^{-1}	slope/ $(cm\ \%)^{-1}$	range/ %	std error/ $(cm\ \%)^{-1}$	intercept/ cm^{-1}	R^2
1.67×10^{-4}	−2.2	0−1.1	0.14	1059.6	0.935
3.33×10^{-4}	−1.8	0−1.2	0.12	1059.3	0.930
8.33×10^{-4}	−2.1	0−1.0	0.07	1059.3	0.992
1.67×10^{-3}	−1.9	0−2.0	0.4	1059.1	0.931

(b) Asymmetric C−C stretching mode band vs applied stress

strain rate/s^{-1}	slope/ $(cm\ GPa)^{-1}$	range/ GPa	std error/ $(cm\ GPa)^{-1}$	intercept/ cm^{-1}	R^2
1.67×10^{-4}	−4.7	0−0.5	0.14	1059.7	0.961
3.33×10^{-4}	−4.1	0−0.7	0.11	1059.5	0.966
5.00×10^{-4}	−3.2	0−0.8	0.10	1058.7	0.985
8.33×10^{-4}	−3.2	0−0.8	0.20	1069.1	0.940
1.67×10^{-3}	−4.5	0−0.8	0.46	1059.0	0.923

Table 6. Dependence of the "Broad" Asymmetric C−C Stretching Mode Band upon Applied Strain or Stress for the Initial Part of the Curve for Which a Linear Fit Was Applied or upon Applied Stress for the Second Part of the Curve for Which a Linear Fit was Applied

(a) "Broad" Asymmetric C−C Stretching Mode Band vs Applied Strain

strain rate/s^{-1}	slope/ $(cm\ \%)^{-1}$	range/ %	std error/ $(cm\ \%)^{-1}$	intercept/ cm^{-1}	R^2
		First Range			
1.67×10^{-4}	−4.6	0−1.1	0.3	1058.7	0.945
3.33×10^{-4}	−3.4	0−1.2	0.5	1059.3	0.809

(b) "Broad" Asymmetric C−C Stretching Mode Band vs Applied Stress

strain rate/s^{-1}	slope/ $(cm\ GPa)^{-1}$	range/ GPa	std error/ $(cm\ GPa)^{-1}$	intercept/ cm^{-1}	R^2
		First Range			
1.67×10^{-4}	−9.8	0−0.5	0.2	1059.4	0.965
3.33×10^{-4}	−7.5	0−0.5	0.6	1060.4	0.750

(c) "Broad" asymmetric C−C stretching mode band vs applied stress

strain rate/s^{-1}	slope/ $(cm\ GPa)^{-1}$	range/ GPa	std error/ $(cm\ GPa)^{-1}$	intercept/ cm^{-1}	R^2
		Second Range			
1.67×10^{-4}	−12.5	0.5−1.5	2.3	1061.3	0.575
3.33×10^{-4}	−18.3	0.5−1.5	2.8	1066.9	0.690

0.6 GPa stress and then at a much higher rate up to 7% strain or 1.7GPa stress just prior to fiber fracture. The Raman data indicate that the abrupt changes occurring at 1.1−1.3% strain or 0.5−0.6 GPa stress and 7% strain or 1.7GPa stress are associated with "yield" points. At the first "yield" point plastic flow of the amorphous material is thought to occur. This brings about (a) a "freeze" and subsequent relaxation of the stresses borne by crystals which are in-series with the plastically deforming amorphous phase and (b) a transfer of stresses by shear to crystals connected in-parallel with the plastically deforming phase. The second "yield" point is possibly associated with the initiation of microcracking which leads to the ultimate failure of the fiber. A number of structural models have been reviewed in the light of the Raman data obtained here.

Acknowledgment. The experimental work was conducted in the Materials Department of Queen Mary & Westfield College (QMW), University of London. Mr. V. Chohan and Dr. A. Paipetis are thanked for assisting with the acquisition of the experimental data. The British Council is thanked for providing P.A.T. Tarantili with a visiting scholarship to QMW.

References and Notes

(1) Smith, P.; Lemstra, P. J. *Macromol. Chem.* **1979**, *180*, 2983.
(2) Prevorsek, D. C.; Chin, H. B.; Murphy, S. *J. Polym. Sci. Polym. Symp.* **1993**, *75*, 81.
(3) Kalb, B.; Pennings, A. J. *Polymer* **1980**, *21*, 3.
(4) Van Hutten, P. E.; Koning C. E.; Pennings, A. J. *J. Mater. Sci.* **1985**, *20*, 1556.
(5) Pennings, A. J. *J. Polym. Sci., Polym. Symp.* **1977**, *58*, 55.
(6) Barham, P. J.; Arridge, R. G. C. *J. Polym. Sci., Polym. Phys.* **1977**, *15*, 1177.
(7) Peterlin, A. In Ultrahigh Modulus Polymers; Cifferi, A., Ward, I. M., Eds.; Applied Science: London, 1979; p 279.
(8) Gibson, A. G.; Davies G. R.; Ward, I. M. *Polymer*, **1978**, *19*, 683.
(9) Takayanagi, M.; Imada, K.; Kajiyama, T. *J. Polym. Sci.* C **1966**, *15*, 263.
(10) Tashiro, K.; Wu, G.; Kobayashi, M. *Polymer* **1988**, *29*, 1768.
(11) Wong, W. F.; Young, R. J. *J. Mater. Sci.* **1994**, *29*, 520.
(12) Holliday, L.; White, J. W. *Pure Appl. Chem.* **1971**, *26*, 545.
(13) He, T. *Polymer* **1986**, *27*, 253.
(14) Galiotis, C.; Young, R. J.; Batchelder, D. N. *J. Polym. Sci., Polym. Phys. Ed.* **1983**, *21*, 2483.
(15) Vlattas, C.; Galiotis, C. *Polymer* **1991**, *32*, 1788.
(16) Melanitis, N.; Galiotis, C. *J. Mater. Sci.* **1990**, *25*, 5081.
(17) Day, R. J.; Robinson, I. M.; Zakikhani, M.; Young, R. J. *Polymer* **1987**, *28*, 1833.
(18) Vlattas, C.; Galiotis, C. *Polymer* **1994**, *35*, 2335.
(19) Prassad, K.; Grubb, D. T. *J. Polym. Sci., Polym. Phys., Ed.* **1989**, *27*, 381.
(20) Kip, B. J.; Van Eijk, M. C. P.; Meier, R. J. *J. Polym. Sci., Polym. Phys. Ed.* **1991**, *29*, 99.
(21) Moonen, J. A. H. M.; Roovers, W. A. C.; Meier, R. J.; Kip, B. J. *J. Polym. Sci. Polym. Phys. Ed.* **1992**, *30*, 361.
(22) Grubb, D. T.; Li, Z. *Polymer* **1992**, *30*, 2587.
(23) Wool, R. P.; Bretzlaff, R. S. *J. Polym. Sci. B* **1986**, *24*, 1039.
(24) Wong, W. F.; Young, R. J. *J. Mater. Sci.* **1994**, *29*, 510.
(25) Paipetis, A.; Vlattas, C.; Galiotis, C. *J. Raman Spectrosc.* **1996**, *27*, 519.
(26) Porter, R. S.; Chuah, H. H.; Kanamoto, T. In *High Modulus Polymers*; Zachariades, A. E., Porter, R. S., Eds.; Marcel Dekker Inc.: New York, 1988; p 259.
(27) Ward, I. M. Mechanical Properties of Solid Polymers, 2nd ed.; John Wiley & Sons: Chichester, England, 1990.
(28) Smook, J.; Hamersma, W.; Pennings, A. J. *J. Mater. Sci.* **1984**, *19*, 1359.
(29) Marichin, V. A.; Mjasnikova, L. P.; Pelzbauer, Z. *J. Macromol. Sci. Phys.* **1983**, *B22*, p 111.
(30) Cox, H. L. *Br. J. Appl. Phys.* **1952**, *3*, 72.

MA961498L